Electrochemistry of Crystalline Mixed Conductors: Concepts and Examples with $SrTiO_3$

J. Jamnik
National Institute of Chemistry, Hajdrihova 19, SI-1000 Ljubljana, Slovenia
Max-Planck Institute fuer Festkoerperforschung,
Heisenbergstr. 1, D-70569 Stuttgart, Germany
janez.jamnik@ki.si

Original scientific paper
Received: October 27, 2006
Accepted: December 22, 2006

The electrochemistry of mixed conductors is outlined. In particular the impact of grain boundaries on the transport perpendicular to the grain boundary plane is studied. Fe-doped $SrTiO_3$ bicrystals were used as prototype mixed conductor. Experimental results obtained by optical spectroscopy (chemical diffusion) and electrochemical impedance spectroscopy (electrical transport) are analysed in terms of continuum models. A unified approach based on the use of "chemical capacitors" is briefly explained. For the description of grain boundary, the Schottky model acting on electronic and ionic charge carriers is used.

Key words:
Mixed conductors, grain boundaries, impedance spectroscopy, chemical diffusion.

Introduction

Mixed conductors are materials in which both ionic and electronic carriers are mobile. Thus, their composition can be varied by an external electrochemical control. This feature qualifies mixed conductors as energy storage media, as materials for electrodes, etc. In contrast to liquid electrolytes, crystalline mixed conductors are in most cases unsupported (only one type of mobile ionic and electronic defects; absence of any supporting electrolyte). Yet, the concentrations of mobile ionic and electronic charge carriers may differ by several orders of magnitude. They can be varied by variation of impurity concentration, by the component partial pressure, temperature and the applied potential. As regards interfacial effects, the existence of internal boundaries introduces important additional materials properties with respect to liquids.

In this paper the interaction of a mixed conductor with external electric and chemical potential perturbations will be considered. Both interactions typically occur, for example, in electrodes used in solid oxide fuel cells, or in insertion materials for energy storage devices. In particular, the impact of surfaces and internal boundaries will be outlined. Experimental results using Fe-doped $SrTiO_3$ bicrystals (prototype mixed conductor) will be given: (i) the electrochemical impedance of the bicrystal comprising $\Sigma 5$ grain boundary (Figs. 2 and 3) and (ii) spatially resolved *in-situ* observation of the chemical diffusion of oxygen through the $\Sigma 13$ grain boundary (Fig. 4) will be discussed. The presentation is given in the form of an overview of previous individual reports.[1–3]

Impact of internal boundaries on mixed conductivity

Internal boundaries can be blocking, highly conductive and can have a distinct transference number (Fig. 1)[3]. There are several possible reasons for distinct transport properties of interfaces: (i) Segregation effect: segregation of impurities and formation of a "third" phase at the interface can make the transfer of carriers across the boundary very sluggish, (ii) Mobility effect: strain induced by the lattice mismatch between two differently ori-

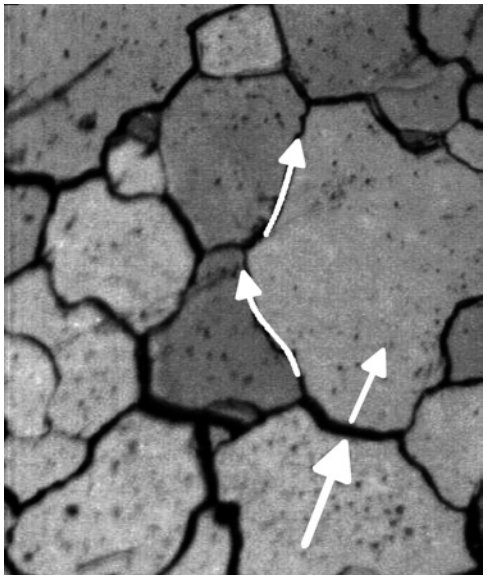

Fig. 1 – *Micrograph of a polycrystalline material. White arrows indicate possible grain boundary effects, as far as the transport is concerned.*

ented grains or two different particles in a composite may lead to a higher mobility of point defects along the grain boundary compared to the bulk. (iii) Concentration effect: Owing to the space charges, local concentration of the carriers within the interfacial zone can be enhanced or decreased compared to the bulk. This way, both the transport along and the transport across the boundary can be modified to a large extent, in particular in materials with relatively low bulk defect density.

Among these three only the latter effect will be discussed in the paper.

As far as experimental methods are concerned, we may emphasise that, in principal, three different methods are available for the study of transport phenomena: (i) Tracer diffusion, (ii) Chemical diffusion and (iii) Electrical transport. Further herein, the latter two will be addressed.

Chemical diffusion: driving force – oxygen partial pressure

In order to reduce the level of complexity, a bicrystal rather than a polycrystalline material is studied (Fig. 2). Fe-doped $SrTiO_3$ has been used in all the experiments. This is a p-type semiconductor. It is nonstoichiometric, oxygen vacancies being the dominant ionic charge carrier. We have chosen this material for the studies of interfacial properties because the bulk materials parameters (dependencies of the mobility and concentrations of the charge carriers on oxygen partial pressure, temperature and

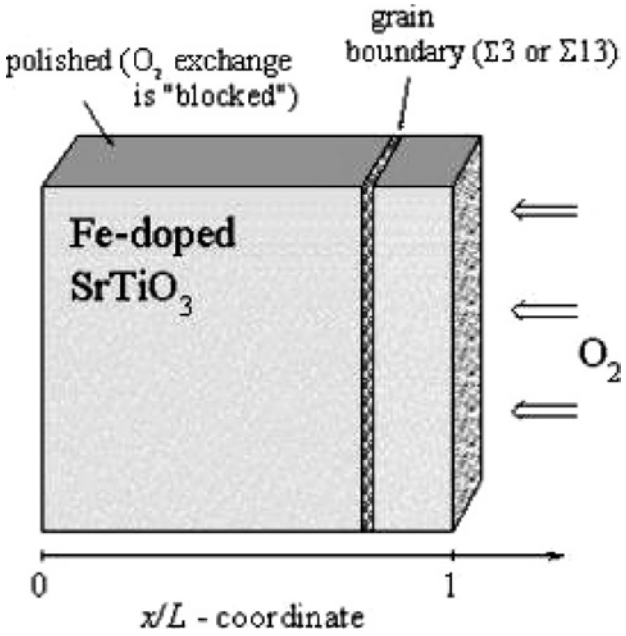

Fig. 2 – *Sketch of the sample's geometry for the chemical diffusion experiment. Surface pre-treatment is indicated as to provide a quasi one-dimensional transport.*

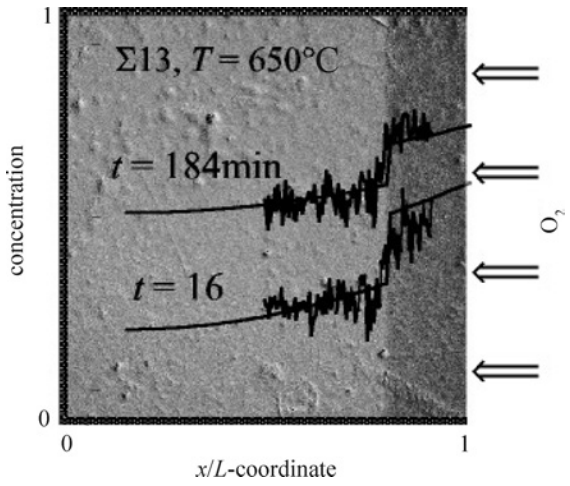

Fig. 3 – *Optical spectroscopy of a bicrystal during in-diffusion of oxygen*

the iron content, see e.g. Ref. (4)) are well known. Experimental details of the experiment are given elsewhere.[1] It is important here that we can prepare a bicrystal such that only one surface is "open" for oxygen exchange, namely the one being parallel to the grain boundary (see Fig. 2). The sample is first equilibrated at given temperature T and oxygen partial pressure (p). Then the partial pressure of oxygen is suddenly enhanced or reduced. The consequent equilibration of the sample is monitored "*in-situ*" and with spatial resolution by optical spectroscopy:[5] an incident laser beam is shined on the crystal surface which is parallel to the direction of the oxygen diffusion and the optical absorption is monitored by a CCD camera placed opposite to the sample. Since we know how optical absorption depends on the ratio of $[Fe^{2+}]$ and $[Fe^{3+}]$ concentrations and, further, how this ratio depends on the concentration of the oxygen vacancies, we are able to monitor the concentration profiles "in-situ" with spatial resolution. A snapshot in the case of the experiment with Σ13 grain boundary is given in Fig. 3. In contrast to Σ3 grain boundary (not shown here) we clearly see a distinct jump of the concentration over the grain boundary. This unambiguously demonstrates the blocking effect of the Σ13 grain boundary on the chemical diffusion.

Electrical transport: driving force – voltage

For the electrical experiment similar bicrystals were used, but this time two identical electrodes were placed on the surfaces parallel to the grain boundary plane.[2] Owing to its excellent reversibility, a thin layer of YBa_2Cu_3 covered by a porous Pt layer was used as electrode material (see insert in Fig. 4).

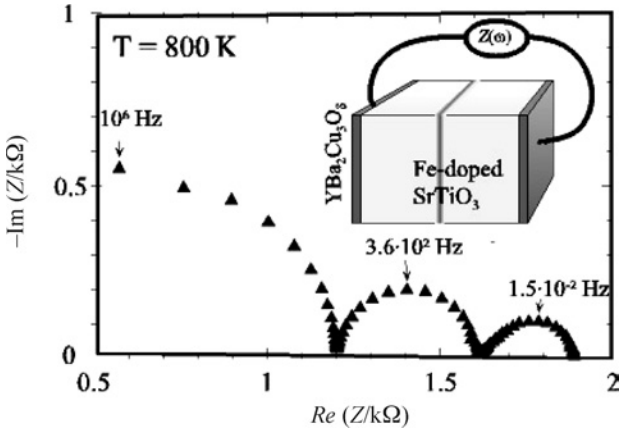

F i g . 4 – *Impedance spectra of Fe-doped $SrTiO_3$ bicrystal*

To check the electrode effects, impedance spectra of a single crystal was measured first. As expected, only one semicircle was observed, which can easily be attributed to the bulk. Although the impedance was measured to frequencies as low as $\nu = 5 \cdot 10^{-5}$ Hz, no electrode response could be detected. Fig. 4 shows the impedance spectra of a bicrystal. Naively, besides the bulk response one also expects a grain boundary semicircle. However, on top of that, we observed an additional feature at very low frequencies, resembling Warburg diffusion. Usually, this type of behaviour is induced by selectively blocking electrodes (i.e. electrodes that are reversible for electronic carriers and blocking for the ionic ones, or vice versa), but in this case the electrode is perfectly reversible for both. Obviously, the diffusion like response is induced by the grain boundary.

Models derived by network thermodynamics

Both experiments can be nicely modelled by the use of network thermodynamics.[6] One starts with commonly accepted transport equations for the mixed conductors. We assume that driving forces are small compared to *kT*. The fluxes are thus proportional to the corresponding gradients of the electrochemical potential, $\nabla\tilde{\mu}_j$. If we neglect the cross terms, one has:

$$\bar{\boldsymbol{J}}_j = -\frac{\sigma_j}{(z_j e)^2}\nabla\tilde{\mu}_j \tag{1}$$

where σ_j is the conductivity of carrier j, z_j is its charge number including sign and e is the absolute value of electronic charge.

In the simplest case we have no internal reactions (internal sources and sinks for the charge carries). Thus the continuity equation reads:

$$\nabla\cdot\bar{\boldsymbol{J}}_j = -\frac{\partial n_j}{\partial t} \tag{2}$$

where n_j is the carrier density.

Since the carriers are charged, we need to take into account Poisson's equation:

$$\nabla^2\phi = -\frac{e}{\varepsilon\,\varepsilon_0}\sum_j z_j n_j \tag{3}$$

where ϕ is the electric potential, ε is the relative dielectric constant and ε_0 is the permittivity of vacuum.

The essence of network thermodynamics is to rewrite the transport equations in terms of fluxes and driving forces. This can be done using a simple, but non-trivial ansatz:

$$\frac{\partial n_j}{\partial t} = \left(\frac{\partial n_j}{\partial \mu_j}\right)_t \frac{\partial \mu_j}{\partial t} + \left(\frac{\partial n_j}{\partial t}\right)_{\mu_j} \tag{4}$$

where μ_j is the chemical potential. The first partial derivative on the right is known as the chemical capacity (please note the similarity with other second derivatives of the Gibbs free energy over the independent variables):

$$C_j \equiv (ez_j)^2\left(\frac{\partial \mu_j}{\partial n_j}\right)^{-1}_{\text{equilibrium}} \tag{5}$$

Then the transport equations (1–3) read (we also replace flux densities with current densities):

$$\vec{I}_j = -\sigma_j\nabla(\mu_j^* + \phi) \tag{6a}$$

$$\nabla\cdot\vec{I}_j = -C_j\frac{\partial}{\partial t}\mu_j^* \tag{6b}$$

$$\vec{I}_{\text{dis}} = -\varepsilon\,\varepsilon_0\frac{\partial}{\partial t}\nabla\phi \tag{6c}$$

Eq. (6a) refers to the dissipation of energy (the flux and the driving force are in phase) while the second and the third equations refer to the pure storage of energy (fluxes and driving forces are out of phase). As we can see, there are two different mechanisms for storage of energy in electrochemistry: dielectric (Eq. (6c)) and chemical (Eq. (6b)). These equations can easily be depicted graphically, that is, as an equivalent circuit (please note that we have one-to-one mapping between the differential equations and the equivalent circuit).

The advantage of the network thermodynamics approach lies in the fact that the general circuit can elegantly be tailored and used for different purposes and experimental set-ups of interest. In the case of

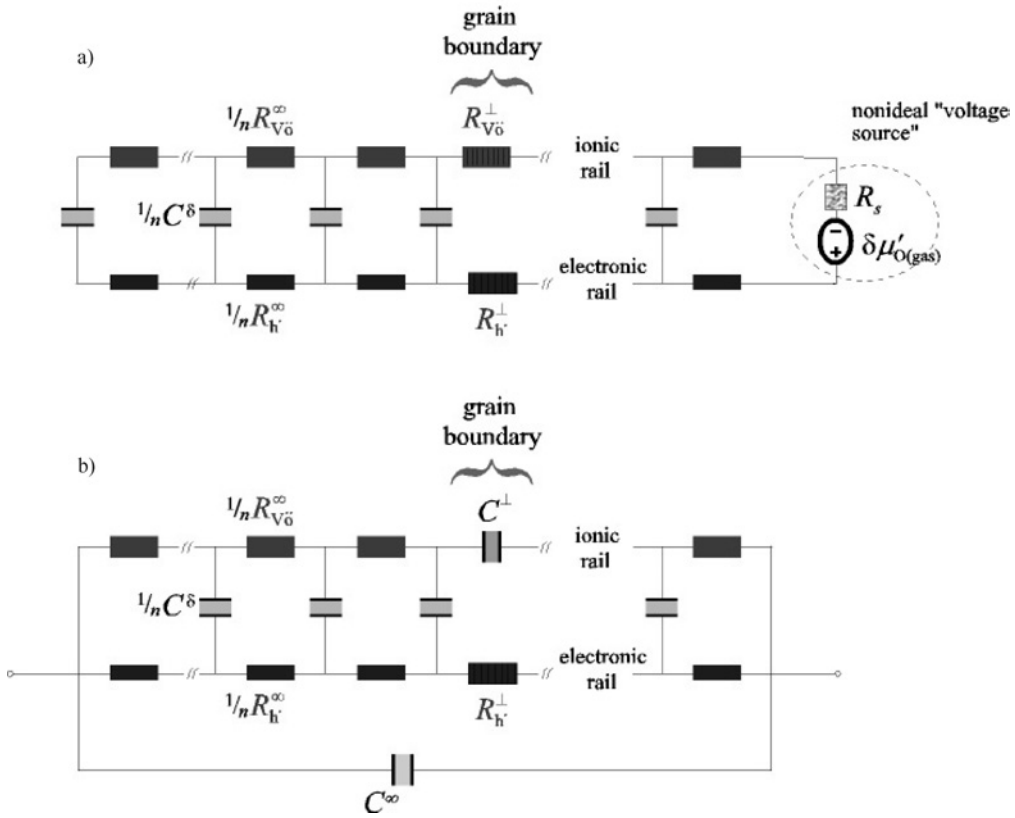

F i g . 5 – *Approximate equivalent circuits for (a) chemical diffusion and (b) electrochemical impedance*

chemical diffusion and impedance under conditions described in the previous two sections, the tailored approximate circuits appear as displayed in Fig 5. The circuit consists of an ionic and electronic rail. The two rails denoted by the resistors $R_{V_O^{\cdot\cdot}}$ and $R_{h^{\cdot}}$, respectively, are coupled by the chemical capacitors C [5]. The superscripts, ∞ and ⊥, refer to the bulk and to the grain boundary, respectively. Symbol n denotes the number of slices into which the whole sample is cut. This parameter is a consequence of discretisation of differential equations and has no meaning in terms of material parameters. Since R's and C's refer to the whole sample, circuit elements are weighted by $1/n$. In derivation we assumed that in the bulk local electroneutrality prevailed (the approximation applies as long as the sample thickness is much larger than the Debye length) and neglected the chemical capacity of the grain boundary (the approximation applies as long as the grain boundary thickness is small compared to grain size). In the case of chemical diffusion (Fig. 5a) we completely neglected all electrostatic capacitances (the time scale of the experiment is far beyond the dielectric relaxation times) and in the case of impedance (Fig. 5b) we neglected the ionic flux across the boundary (we know from different experiments that ionic resistance of the boundary is higher than the electronic resistance).

The validity of the model is demonstrated in Fig. 3 for the chemical diffusion and in Fig. 6 for

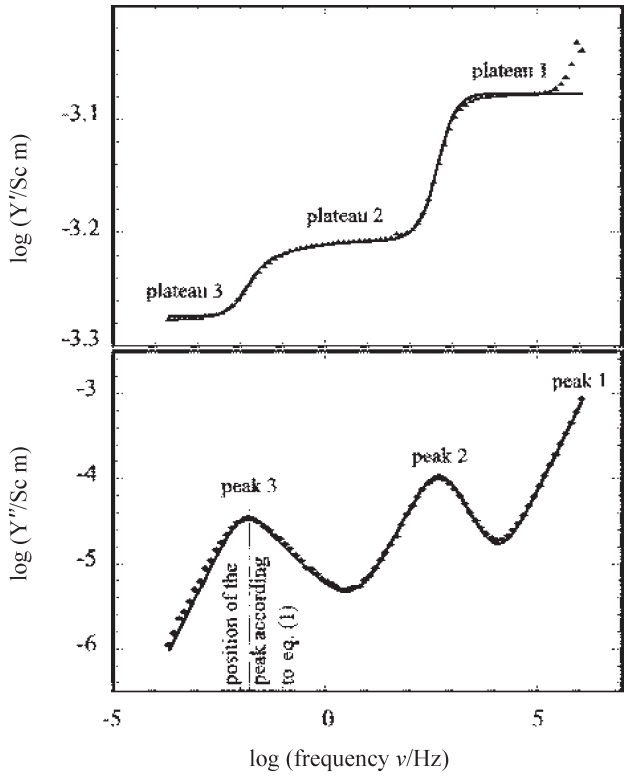

F i g . 6 – *Impedance spectra shown as real and imaginary part of the admittance as the function of frequency. Symbols refer to the measurements and solid lines to the fit*

impedance spectroscopy. Please note that all the fit parameters referring to the bulk were verified by comparison with other experiments made on single crystals and the agreement is very good. As far as the interface is concerned, only one fitting parameter was used, *i.e.*, the height of the Schottky barrier.[7,8] Obviously, the results show (i) the applicability of the model to different type of experiments (different external driving forces), and (ii) the applicability of the Schottky barrier model for the electrons and ions. Please note that the two experiments shown are differently sensitive to the ionic and electronic transport coefficient of the barrier. While in the case of chemical diffusion the carrier with the lowest "effective" σ prevails, just the opposite is true in the case of electrochemical impedance.

Summary and conclusions

Two examples of precise measurements of chemical diffusion and electrochemical impedance of a $SrTiO_3$ bicyrstal are shown. The blocking, or more precisely, the selectively blocking properties of the $\Sigma 5$ and $\Sigma 13$ grain boundaries were clearly detected. The measured results can be modelled in a general way using network thermodynamics. Both measurements can be consistently explained if one assumes the Schottky model for the grain boundary, which acts both on the electronic on the ionic charge carriers.

References

1. *Jamnik, J., Guo, X., Maier, J.*, Appl. Phy. Lett. **82** (2003) 2820.
2. *Leonhartd, M., Jamnik, J., Maier, J.*, Electrochem. Solid St. **2** (1999) 333.
3. *Jamnik, J., Maier, J.*, Solid State Ionics **119** (1999) 191.
4. *Denk, I., Noll, F., Maier, J.*, J. Am. Ceram. Soc. **80** (1997) 279.
5. *Bieger, T., Maier, J., Waser, R.*, Ber. Bunsen-Ges. Phys. Chem. **97** (1993) 1098.
6. *Jamnik, J., Maier, J.*, Phys. Chem. Chem. Phys. **3** (2001) 1668.
7. *Balaya, P., Jamnik, J., Fleig, J., Maier, J.*, Appl. Phy. Lett. **88** (2006) art no. 62109.
8. *Waser, R.*, Ferroelectrics **133** (1992) 109.